ISSN 0023-1584, Kinetics and Catalysis, 2008, Vol. 49, No. 2, pp. 261–270. © MAIK "Nauka/Interperiodica" (Russia), 2008.
Original Russian Text © I.S. Yakovleva, L.A. Isupova, V.A. Rogov, V.A. Sadykov, 2008, published in Kinetika i Kataliz, 2008, Vol. 49, No. 2, pp. 274–283.

Forms of Oxygen in $La_{1-x}Ca_xMnO_{3+\delta}$ (x = 0–1) Perovskites and Their Reactivities in Oxidation Reactions

I. S. Yakovleva, L. A. Isupova, V. A. Rogov, and V. A. Sadykov

Boreskov Institute of Catalysis, Siberian Branch, Russian Academy of Sciences, Novosibirsk, 630090 Russia
e-mail: irga@catalysis.ru

Received November 14, 2006

Abstract—The effects of substitution in the cationic sublattice and of the synthesis procedure on the reactivity of different forms of oxygen in $La_{1-x}Ca_xMnO_{3+\delta}$ perovskites synthesized by mechanochemical and ceramic processing was studied by temperature-programmed reduction (TPR) with hydrogen. As the calcium content of the perovskite is raised, the maxima of the TPR peaks shift to lower temperatures and the extent of reduction of the perovskite increase, implying an increase in the reactivity of the system. Conversely, raising the calcination temperature or extending the calcination time shifts the maxima of the peaks to higher temperatures and diminishes the extent of reduction of the sample. TPR data for the intermediate-composition samples can be explained in terms of the dependence of microstructure on the synthesis procedure (near-surface calcium segregation in the mechanochemically synthesized samples and the microheterogeneous structure of the ceramic samples). The reduction process $Mn^{4+} \longrightarrow Mn^{2+}$ takes place in the low- and medium-temperature regions. According to the literature, the bulk reduction process $Mn^{3+} \longrightarrow Mn^{2+}$ occurs at high temperatures. The activity of the system in CO oxidation is correlated with the amount of the most reactive surface oxygen, which is eliminated in hydrogen TPR runs below 250–300°C.

DOI: 10.1134/S0023158408020146

INTRODUCTION

At present, numerous studies are devoted to the physicochemical properties of mixed oxides with a perovskite structure ((RE)(TE)O_3, where RE = rare-earth cation and TE = transition element cation) [1–3]. The keen interest in these perovskites, particularly substituted perovskites with the general formula $(RE)_{1-x}(AE)_xTEO_3$ (AE = alkaline-earth element: Ca, Sr, Ba), is due to their uncommon electronic, magnetic, and transport properties. Among the perovskite series, the manganites $(RE)_{1-x}(AE)_xMnO_3$ have received special attention, which possess unique ferromagnetic and antiferromagnetic properties [4–6]. Furthermore, they are among the most active thermally stable catalysts usable in various processes [7, 8]. There have been numerous publications concerning the catalytic properties of manganites. They have primarily dealt with the total and partial hydrocarbon oxidation [8] and the burning of CO and other toxic gases [9–11]. The substituted manganites $(RE)_{1-x}(AE)_xMnO_3$ are widely known for their colossal magnetoresistance, which makes them promising functional materials for microelectronics [5, 12]. Furthermore, the high-temperature oxygen and electron conductivity of these materials, along with their catalytic properties, opens great prospects for use of substituted manganites as cathode materials in fuel cells [13, 14].

Earlier, we studied the phase composition, real structure, and catalytic properties of the $La_{1-x}Ca_xMnO_{3+\delta}$ system prepared by conventional ceramic processing using mechanochemical pretreatment before the heat treatment stage (so-called mechanochemical method) [15]. This new, fast, almost wasteless method allowed us to shorten the synthesis time from tens or even hundreds of hours to 3–4 h and to reduce the synthesis temperature from 1100–1200 to 900–1100°C.

It was found that the ceramic synthesis of $La_{1-x}Ca_xMnO_{3+\delta}$ yields calcium solid solutions based on the perovskite structure [15]. The mechanochemical method yields solid solutions up a calcium content of x = 0.4; the materials with higher calcium contents are heterophase and have the structure of a microheterogeneous composite.

The catalytic properties of the system were studied in CO oxidation as a model reaction. It was found that the specific catalytic activity (SCA) of the system varies nonmonotonically as calcium is progressively substituted for lanthanum [15]. The fact that SCA passes through a minimum at medium extents of calcium substitution was explained by the surface segregation of calcium (based on SIMS data) and by the possible blocking of part of the active sites on the surface. The next step in this investigation should be a study of the reactivity and proportions of the forms of oxygen in this perovskite series. Such studies are usually carried out by temperature-programmed reduction (TPR) with hydrogen.

The literature concerning the hydrogen TPR of manganites indicates that there are different forms of oxygen in the $La_{1-x}(AE)_xMnO_{3+\delta}$ perovskites and that these forms differ in their amount and reactivity, and different reduction mechanisms are suggested for unsubstituted and substituted manganites [16–18]. Reports dealing with the hydrogen TPR of unsubstituted manganites (including supported manganites) usually distinguish two main TPR peaks, namely, the low-temperature peak arising from the reduction process $Mn^{4+} \longrightarrow Mn^{3+}$ ($T_{max} \sim 435$°C [17]) and the high-temperature peak corresponding to the process $Mn^{3+} \longrightarrow Mn^{2+}$ accompanied by perovskite decomposition [16–18]. Substituted manganites are characterized by more complicated TPR profiles with split peaks. For example, Ponce et al. [18] attribute the low-temperature reduction of $La_{1-x}Sr_xMnO_{3-y}$ (peak at $T \sim$ 430°C) to the reduction of Mn^{4+} to Mn^{3+}. They explain the observed peak splitting by the difference between the forms of oxygen in the coordination spheres of the Mn^{4+} cations resulting from the substitution of divalent strontium for trivalent lanthanum (type 1) and the Mn^{4+} cations that are due to the existence of cationic vacancies in the lanthanum sublattice (type 2).

Ciambelli et al. [16] also observed that the introduction of strontium into the $La_{1-x}Sr_xMnO_{3-y}$ system causes TPR peak splitting. Furthermore, they observed an increased hydrogen uptake at the low-temperature peaks and attributed this effect to the deeper reduction process $Mn^{4+} \longrightarrow Mn^{2+}$, which, in the authors' opinion, could be due to the disorder in the substituted perovskite structure. In the high-temperature TPR region, they, like other authors, observed the reduction process $Mn^{3+} \longrightarrow Mn^{2+}$ accompanied by the breakdown of the perovskite structure into simple oxides (MnO, La_2O_3, and SrO) and water.

Thus, based on previous reports [16–18], one can expect the existence of at least three forms of oxygen in the substituted manganites: oxygen from the coordination sphere of Mn^{3+} and two forms of oxygen from the coordination sphere of Mn^{4+}, one having a calcium ion as a neighbor (hereafter, $O_{Mn^{4+}-Ca}$) and the other having no such calcium ion (hereafter, the "overstoichiometric" form O_δ). Accordingly, the two forms of highly charged manganese cation Mn^{4+} will be designated Mn^{4+}_{La} (the manganese form that is due to the presence of the overstoichiometric oxygen O_δ) and Mn^{4+}_{Ca} (the manganese form compensating for the charge lost upon the introduction of calcium). Note that only samples with low degrees of substitution ($0 \le x \le 0.5$) were examined in previous works [16, 18]. We failed to find any information concerning the forms of oxygen and their amounts for the whole series of substituted perovskites. In our earlier studies of substituted ferrite–perovskite systems $La_{1-x}Ca_xFeO_{3-y}$ and $La_{1-x}Sr_xFeO_{3-y}$ [19, 20], we established a correlation between the catalytic activity of the oxides in CO oxidation and the amount of the least strongly bound surface oxygen. Therefore, for the substituted manganite series considered here, it is necessary to examine TPR temperatures below 300°C, which may be the temperature region in which this form of oxygen is eliminated.

The above analysis prompted us to characterize the $La_{1-x}Ca_xMnO_{3+\delta}$ perovskites by hydrogen TPR, to reveal the forms of oxygen present in these materials, and to determine their amounts as a function of the chemical composition and preparation procedure. Furthermore, we will report the correlation of the catalytic properties of the oxides in CO oxidation with the oxidation state of the oxygen–manganese subsystem and with the amount of the least strongly bound surface oxygen.

EXPERIMENTAL

The starting compounds were the simple oxides La_2O_3, CaO, and MnO_2 (reagent grade).

In the mechanochemical synthesis of $La_{1-x}Ca_xMnO_{3+\delta}$ (x = 0, 0.2, 0.4, 0.6, 0.8, 1), a mechanically preactivated mixture containing appropriate proportions of the starting oxides was calcined at 900 or 1100°C for 4 h. The mechanical treatment time was 10 min. The mechanical synthesis procedure was described in an earlier work [15]. Ceramic synthesis was carried out by calcination of mixtures of the starting oxides at 1100°C for 100 h (for details, see [15]). The most important phase composition and specific surface area data for the $La_{1-x}Ca_xMnO_{3+\delta}$ samples of the ceramic and mechanochemical (MC) series [15] are listed in Tables 1–3.

Catalytic activity in CO oxidation was measured at 200–450°C in a circulating flow reactor for a catalyst particle size fraction of 0.5–1 mm. The reaction products were identified chromatographically. A detailed description of catalytic tests is presented elsewhere [15].

Hydrogen TPR experiments were carried out for the 0.25–0.50 mm size fraction in a flow reactor fitted with a thermal-conductivity detector. Before being reduced, the samples were conditioned in O_2 at 500°C for 0.5 h and were then cooled to room temperature in O_2. The sample weight was 50 mg, and the flow rate of the reducing mixture (10% H_2 in Ar) was 40 cm^3/min. The samples were heated at a rate of 10 K/min to 900°C. The error of the determination of the component concentrations in the mixture did not exceed 20%. The TPR peak areas, which were a measure of hydrogen uptake (mmol/(g sample)), were determined using the Origin 6.0 program.

Table 1. Phase composition and phase stoichiometry of ceramic $La_{1-x}Ca_xMnO_{3+\delta}$ samples

x	Phase composition[a], %	Formula of the phase[b]	Mn^{4+}, %[c]	Mn^{3+}, %[d]
0	$LaMnO_{3+\delta}$(95.0), Mn_3O_4(3.0)	$La(Mn_{0.16})^{4+}(Mn_{0.84})^{3+}O_{3.08}$	16	91
0.2	$La_{0.8}Ca_{0.2}MnO_{3+\delta}$(97.0), $LaMnO_{3+\delta}$(~1), Mn_3O_4(0.1)	$La_{0.8}Ca_{0.2}(Mn_{0.24})^{4+}(Mn_{0.76})^{3+}O_{3.02}$	22	80
0.4	$La_{0.6}Ca_{0.4}MnO_{3+\delta}$(91.0), $LaMnO_{3+\delta}$(5.3), Mn_3O_4(0.03)	$La_{0.6}Ca_{0.4}(Mn_{1.03})^{4+}O_{3.36}$	75	68
0.6	$La_{0.4}Ca_{0.6}MnO_{3+\delta}$(92.2), $LaMnO_{3+\delta}$(3.23), Mn_3O_4(0.3)	$La_{0.4}Ca_{0.6}(Mn_{0.58})^{4+}(Mn_{0.42})^{3+}O_{2.99}$	62 (1 + 2)	33
0.8	$La_{0.2}Ca_{0.8}MnO_{3+\delta}$(91.2), Mn_3O_4(1.6)	$La_{0.2}Ca_{0.8}(Mn_{0.82})^{4+}(Mn_{0.18})^{3+}O_{3.01}$	80	24 (2 + 3)
1.0	$CaMnO_{3-\delta}$(95.8)[e], Mn_3O_4(3.5)	$Ca(Mn_{0.92})^{4+}(Mn_{0.08})^{3+}O_{2.96}$ ($Ca(Mn_{0.92})^{4+}(Mn_{0.08})^{3+}O_{2.96}$(58%), $Ca_2Mn_2O_5$(38%)	97	

[a] The cation stoichiometry is derived from differentiating dissolution data [15].
[b] The nonstoichiometric oxygen content (δ) is calculated from total hydrogen uptake data; manganese cation ratio, from the electroneutrality condition.
[c] The Mn^{4+} content (in percent of the total manganese content) is calculated from hydrogen uptake at the first peak or from total hydrogen uptake at the first two peaks (the latter case is designated (1 + 2)).
[d] The Mn^{3+} content (in percent of the total manganese content) is calculated from hydrogen uptake at the second peak or from the total hydrogen uptake at the peaks above 600°C (the latter case is designated (2 + 3)).
[e] For the x = 1 samples of all three series, the total percentage of perovskite $CaMnO_3$ and braunmillerite $Ca_2Mn_2O_5$ is presented (according to X-ray diffraction data).

Table 2. Phase composition and phase stoichiometry of mechanochemical $La_{1-x}Ca_xMnO^*_{3+\delta}$ samples at T_{calcin} = 900°C

x	Phase composition, %	Formula of the phase	Mn^{4+}, %	Mn^{3+}, %
0	$LaMnO_{3+\delta}$(94.0), Mn_3O_4(2.4)	$La(Mn_{0.24})^{4+}(Mn_{0.76})^{3+}O_{3.12}$	23	77
0.2	$La_{0.8}Ca_{0.2}MnO_{3+\delta}$(69.0), $LaMnO_{3+\delta}$(6.0), Mn_3O_4(7.8)	$La_{0.8}Ca_{0.2}(Mn_{0.66})^{4+}(Mn_{0.34})^{3+}O_{3.23}$	66	36
0.4	$La_{0.6}Ca_{0.4}MnO_{3+\delta}$(75.0), Mn_3O_4(2.0)	$La_{0.6}Ca_{0.4}(Mn_{0.76})^{4+}(Mn_{0.24})^{3+}O_{3.18}$	72 (1 + 2)	31
0.6	$La_{0.4}Ca_{0.6}MnO_{3+\delta}$(66.0), $CaMnO_{3-\delta}$(12.4), Mn_3O_4(4.2)	$La_{0.4}Ca_{0.6}(Mn_{0.80})^{4+}(Mn_{0.20})^{3+}O_{3.10}$	80 (1 + 2 + 3)	14.4
0.8	$La_{0.4}Ca_{0.6}MnO_{3+\delta}$(60.0), $CaMnO_{3-\delta}$(28.0), Mn_3O_4(4.2)	$La_{0.2}Ca_{0.8}(Mn_{0.78})^{4+}(Mn_{0.22})^{3+}O_{2.99}$	80	20 (2 + 3)
1.0	$CaMnO_{3-\delta}$(84.5), Mn_3O_4(2.3)	$Ca(Mn_{0.90})^{4+}(Mn_{0.10})^{3+}O_{2.95}$	93	

Note: Calcination conditions: T = 900°C, 4 h.
* See notes to Table 1.

Table 3. Phase composition and phase stoichiometry of mechanochemical $La_{1-x}Ca_xMnO^*_{3+\delta}$ samples at T_{calcin} = 1100°C

x	Phase composition, %	Formula of the phase	Mn^{4+}, %	Mn^{3+}, %
0	$LaMnO_{3+\delta}$(96.1), Mn_3O_4(2.8)	$La(Mn_{0.2})^{4+}(Mn_{0.8})^{3+}O_{3.1}$	20	80
0.2	$La_{0.8}Ca_{0.2}MnO_{3+\delta}$(92.1), Mn_3O_4(1.9)	$La_{0.8}Ca_{0.2}(Mn_{0.28})^{4+}(Mn_{0.72})^{3+}O_{3.04}$	29	70
0.4	$La_{0.6}Ca_{0.4}MnO_{3+\delta}$(86.0), $CaMnO_{3-x}$(4.0), Mn_3O_4(2.2)	$La_{0.6}Ca_{0.4}(Mn_{0.46})^{4+}(Mn_{0.54})^{3+}O_{3.03}$	54	40
0.6	$La_{0.6}Ca_{0.4}MnO_{3+\delta}$(40.0), $La_{0.2}Ca_{0.8}MnO_{3+\delta}$(37.0), $CaMnO_{3-x}$(20.0), Mn_3O_4(0.3)	$La_{0.4}Ca_{0.6}(Mn_{0.42})^{4+}(Mn_{0.58})^{3+}O_{2.91}$	67 (1 + 2)	40
0.8	$La_{0.6}Ca_{0.4}MnO_{3+\delta}$(20.0), $La_{0.22}Ca_{0.83}MnO_{3+\delta}$(50.0), $CaMnO_{3-x}$(25.0), Mn_3O_4(0.7)	$La_{0.2}Ca_{0.8}(Mn_{0.72})^{4+}(Mn_{0.18})^{3+}O_{2.96}$	78	22 (2 + 3)
1.0	$CaMnO_{3-x}$(93.4), Mn_3O_4(0.4)	$Ca(Mn_{0.82})^{4+}(Mn_{0.18})^{3+}O_{2.91}$ $Ca(Mn_{0.90})^{4+}(Mn_{0.10})^{3+}O_{2.95}$(54%), $Ca_2Mn_2O_5$(39%)	90	–

Note: Calcination conditions: T = 1100°C, 4 h.
* See notes to Table 1.

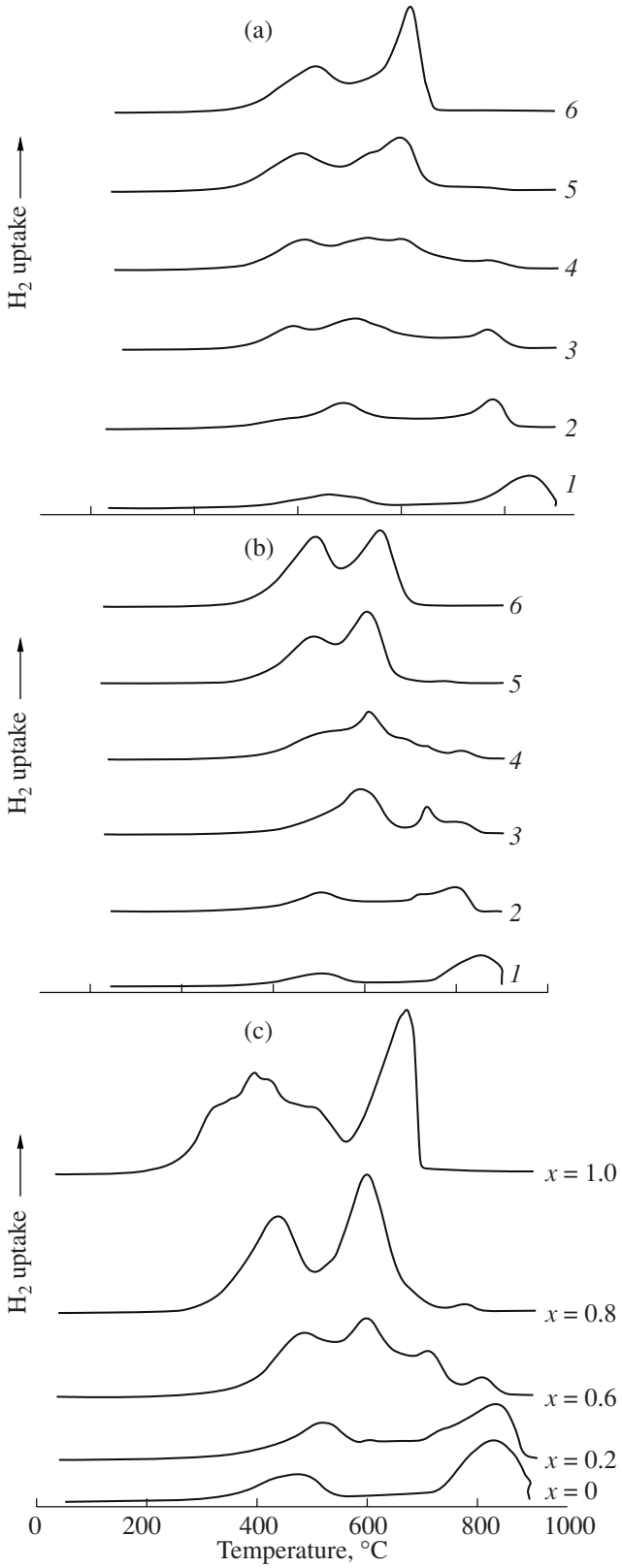

Fig. 1. TPR profiles for $La_{1-x}Ca_xMnO_{3+\delta}$ perovskites with x = (*1*) 0, (*2*) 0.2, (*3*) 0.4, (*4*) 0.6, (*5*) 0.8, and (*6*) 1.0: (a, b) mechanochemical series (T_{calcin} = (a) 900 and (b) 1100°C); (c) ceramic series.

RESULTS

Tentative Scheme of the Temperature-Programmed Reduction of the System and Phase Formulas Calculated from TPR Data

Figure 1 plots hydrogen uptake versus the reduction temperature for different extents of substitution (x) and different sample preparation conditions (calcination temperature and time). Each TPR curve has at least two peaks, which correspond to the elimination of two different forms of oxygen. The TPR curves of the substituted perovskites $La_{1-x}Ca_xMnO_{3+\delta}$ are more complicated than the curves of the terminal members of the series ($LaMnO_{3+\delta}$ and $Ca_xMnO_{3-\delta}$). For example, the TPR curves of the $LaMnO_{3+\delta}$ samples have two peaks, which correspond to the manganese reduction processes $Mn^{4+} \longrightarrow Mn^{2+}$ and $Mn^{3+} \longrightarrow Mn^{2+}$ (see below). As the calcium content x is increased, the peaks split and/or broaden and their maxima shift to lower temperatures. This is accompanied by an increase in the total hydrogen uptake, which indicates an increase in the degree of reduction of the samples. Table 4 lists quantitative hydrogen uptake data for the $La_{1-x}Ca_xMnO_{3+\delta}$ series.

Our preliminary calculations of the Mn^{4+} and Mn^{3+} fractions from the total hydrogen uptake (the total amount of hydrogen consumed by the end of the TPR run) and the hydrogen uptake at the high-temperature peak demonstrated that, as the calcium content is raised, the Mn^{4+} fraction increases and the Mn^{3+} fraction decreases (Tables 1–3). This finding allowed us to assume that the deeper reduction $Mn^{4+} \longrightarrow Mn^{2+}$ can take place even in the low-temperature region. Indeed, the Mn^{4+} content calculated from the uptake at the low-temperature peaks is nearly equal to the Mn^{4+} content deduced from the total uptake data under the assumption that the deeper reduction process takes place in the low-temperature region. The exceptions are the $x = 0.8$ samples, for which the Mn^{3+} content derived from the high-temperature peak areas is close to 100%. This is possible only if the less deep reduction process, $Mn^{4+} \longrightarrow Mn^{3+}$, takes place in the low-temperature region.

Based on the literature [16–20] discussed in the Introduction and on the preliminarily calculated Mn^{4+} and Mn^{3+} contents, we will consider the following four hydrogen uptake regions in order to assign TPR peaks to particular oxygen elimination/manganese cation reduction processes:

(1) low-temperature region (up to 300°C), where the hydrogen uptake corresponds to the elimination of no more than one oxygen monolayer from the surface;

(2) modest-temperature region (370–500°C), in which excess oxygen is removed from the coordination sphere of the Mn^{4+}_{La} cations so that the amount of oxygen eliminated corresponds quantitatively to the process $Mn^{4+} \longrightarrow Mn^{2+}$;

Table 4. Hydrogen TPR data for samples prepared in different ways

Composition (x)	T_{max} for TPR peaks, °C (hydrogen uptake × 10^3, (mol H_2)/g) Σ = total hydrogen uptake × 10^3, (mol H_2)/g			Reduction process
	MC series (T_{calcin} = 900°C, 4 h)	MC series (T_{calcin} = 1100°C, 4 h)	ceramic series	
0	457 (0.89) 848 (1.5) Σ = 2.40	504 (0.79) 849 (1.36) Σ = 2.35	478 (0.78) 830 (1.43) Σ = 2.35	$Mn^{4+} \longrightarrow Mn^{2+}$ $Mn^{3+} \longrightarrow Mn^{2+}$
0.2	370 (0.36) 488 (1.71) 738 (1.09) Σ = 2.84	– 504 (1.23) 794 (1.47) Σ = 2.73	– 519 (0.98) 834 (1.80) Σ = 2.78	Elimination of O_δ inserted in interblock boundaries $Mn^{4+} \longrightarrow Mn^{2+}$ $Mn^{3+} \longrightarrow Mn^{2+}$
0.4	393 (0.84) 510 (1.85) 768 (0.58) Σ = 3.40	– 587 (2.56) 734 (0.53) 807 (0.31) Σ = 3.43	378 (2.27) 483 (1.1) 641 (1.51) 767 (0.92) Σ = 4.99	Elimination of O_δ inserted in interblock boundaries $Mn^{4+} \longrightarrow Mn^{2+}$ $Mn^{3+} \longrightarrow Mn^{2+}$
0.6	415 (1.39) 534 (1.19) 595 (1.19) 770 (0.26) Σ = 4.01	469 (0.67) 532 (0.65) 609 (1.6) 736 (0.65) 810 (0.20) Σ = 3.89	482 (1.68) 600 (1.56) 708 (0.62) 809 (0.22) Σ = 4.06	$Mn^{4+} \longrightarrow Mn^{2+}$ $Mn^{4+} \longrightarrow Mn^{3+}, Mn^{2+}$ $Mn^{3+} \longrightarrow Mn^{2+}$
0.8	409 (2.01) 597 (2.49) 723 (0.12) Σ = 4.66	487 (2.26) 605 (2.65) 771 (0.06) Σ = 4.97	433 (2.17) 600 (2.78) 776 (0.08) Σ = 4.98	$Mn^{4+} \longrightarrow Mn^{3+}$ (except for the MC sample calcined at 900°C) $Mn^{3+} \longrightarrow Mn^{2+}$ $Mn^{3+} \longrightarrow Mn^{2+}$
1.0	437 (2.41) 620 (5.59) Σ = 5.59	492 (3.41) 634 (3.09) Σ = 6.45	398 (3.99) 873 (2.62) Σ = 6.63	$Mn^{4+} \longrightarrow Mn^{2+}$ $Mn^{3+} \longrightarrow Mn^{2+}$

(3) medium-temperature region (440–600°C), in which oxygen is removed from the coordination sphere of the Mn_{Ca}^{4+} cations so that the amount of oxygen eliminated again corresponds quantitatively to the process $Mn^{4+} \longrightarrow Mn^{2+}$ ($Mn^{4+} \longrightarrow Mn^{3+}$ for the $x = 0.8$ samples calcined at 1100°C);

(4) high-temperature region (>600°C), in which the process $Mn^{3+} \longrightarrow Mn^{2+}$ occurs and the perovskite structure breaks down to yield MnO.

Tables 1–3 list oxygen content and highly charged manganese cation content data for the $La_{1-x}Ca_xMnO_{3+\delta}$ samples derived from the total amount of hydrogen consumed by the end of the TPR run (and the oxide electroneutrality condition) and, for comparison, the same data derived from the hydrogen uptake at the TPR peaks that we assigned to the reduction of Mn^{4+} to Mn^{2+}. The data presented in the tables for Mn^{4+} were calculated under the assumption that the oxides are single-phase; however, this is not always true (see the second column, which lists phase composition data determined by the differentiating dissolution (DD) data). The Mn^{4+} contents derived from the total hydrogen consumption and the same data calculated from the area of the corresponding peak are in good agreement for single-phase samples. In the other cases, when the sample is not single-phase (MC series) or is single-phase but microheterogeneous (ceramic series), these calculations are discrepant. This fact suggests that part of the oxygen assigned to Mn^{4+} reduction (based on total hydrogen consumption data) is not necessarily bound to Mn^{4+} cations. This amount of oxygen might occur, for example, at phase boundaries.

Thus, based on the simultaneous analysis of TPR and phase composition data (Tables 1–3), we suggest the following model of the reduction of the perovskites with hydrogen (Table 4, Fig. 2): the reduction process $Mn^{4+} \longrightarrow Mn^{2+}$ takes place below 600°C, and the pro-

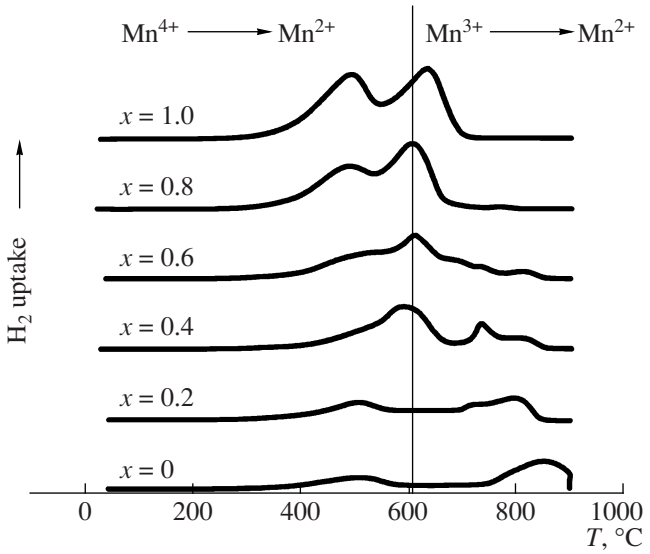

Fig. 2. Reduction scheme for the mechanochemical $La_{1-x}Ca_xMnO_{3-y}$ samples calcined at 1100°C for 4 h.

cess $Mn^{3+} \longrightarrow Mn^{2+}$ begins above 600°C. The exceptions are the $x = 0.8$ samples, for which the first peak arises from the less deep reduction process $Mn^{3+} \longrightarrow Mn^{2+}$ (further studies are required to understand why these samples are more stable), as well the $x = 0.6$ samples, in which the reduction processes occur almost simultaneously and are, therefore, difficult to separate. Furthermore, our data indicate that the existence and reactivity of different forms of oxygen in the $La_{1-x}Ca_xMnO_{3+\delta}$ oxides depend both on the oxide composition and on the synthesis conditions.

Composition Effect

As the calcium content is increased, the reducibility of the perovskite increases: for example, the bulk reduction of lanthanum manganite begins at 700°C (giving rise to a peak at 830–850°C, depending on the sample series), while the reduction of calcium manganite is almost complete at this temperature. Because the maxima of the peaks shift as the calcium content x is increased, the division of the entire TPR temperature ranges into the modest-, medium-, and high-temperature regions is rather arbitrary. For this reason, we will consider the data obtained in this study in greater detail.

Hydrogen uptake in the low-temperature region (up to 300°C). This region is distinguished for the reason that the amount of oxygen eliminated is no larger than one monolayer on the surface. This corresponds to the removal of the least strongly bound, the most reactive forms of oxygen. According to our calculations, the dependence of the hydrogen uptake on x in this region is nonmonotonic and has a minimum at intermediate compositions ($x \sim 0.5$). This finding correlates well

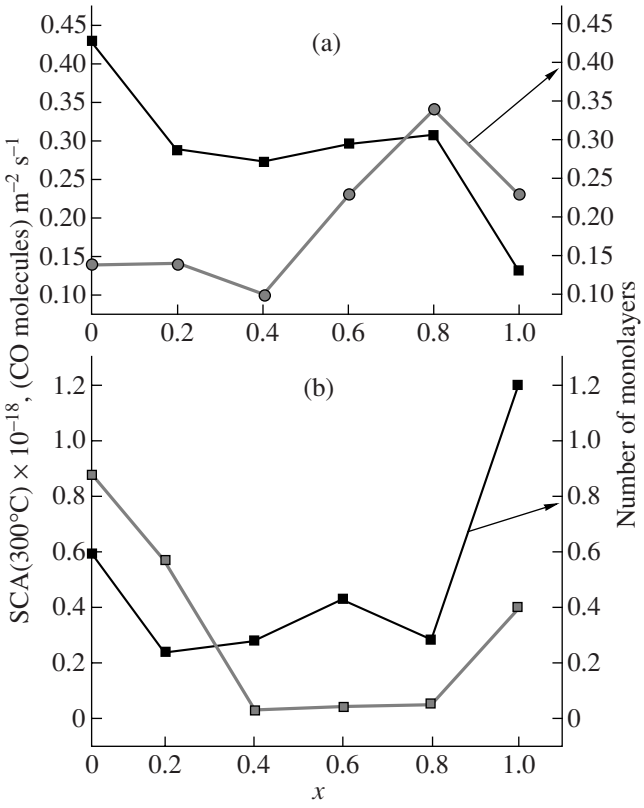

Fig. 3. CO oxidation rate at $T_{test} = 300$°C and the amount of weakly bound oxygen (the number of monolayers removed by hydrogen TPR below 300°C) as a function of the sample composition (x) for the mechanochemical samples calcined at T = (a) 900 and (b) 1100°C.

with the way the catalytic activity of the system varies with the extent of substitution (Fig. 3).

Hydrogen uptake giving rise to peaks in the modest-temperature region (370–500°C). In this temperature range, hydrogen reduces the Mn^{4+}_{La} cations, which have "overstoichiometric" oxygen O_δ in their coordination spheres.

The fact that unsubstituted lanthanum manganite contains Mn^{4+} cations due to "overstoichiometric" oxygen is well known from the literature ($LaMnO_{3.15}$ [4], $LaMnO_{3.19}$ [21]). Furthermore, the Mn^{4+} content (and, accordingly, the "overstoichiometric" oxygen content) depends on the chemical composition of the sample, in particular, on the presence of substituting cations. For example, in the $La_{1-x}Sr_xMnO_{3-y}$ system [19], the Mn^{4+} fraction compensating for the "overstoichiometric" oxygen decreases with increasing strontium content, while the total Mn^{4+} content compensating for the decrease in electric charge increases as strontium is progressively introduced (see TPR data). Our data for the samples calcined at the higher temperature (ceramic and MC series, $T_{calcin} = 1100$°C; see Tables 1 and 3) indicate that the amount of "overstoichiometric" oxygen changes nonmonotonically as calcium is intro-

duced and passes through a minimum at intermediate calcium contents. This finding is in agreement with the results of our earlier study [19]. For the samples calcined at the lower temperature, the calculated "overstoichiometric" oxygen (Table 2) fraction increases monotonically with increasing calcium content.

Thus, according to our data, hydrogen uptake in the modest-temperature region is quantitatively consistent with the $Mn^{4+} \longrightarrow Mn^{2+}$ process. This is in agreement with the results reported by Cimino et al. [17] and is at variance with the inference that the less deep reduction process $Mn^{4+} \longrightarrow Mn^{3+}$ takes place [16, 18]. It was demonstrated that the extent of reduction of the samples in the modest-temperature region depends on the synthesis conditions (the defect structure of the sample). This point needs further investigation. Note, for example, the abnormally high hydrogen uptake by the ceramic sample with x = 0.4 in the low-temperature region (the corresponding curve is not presented in Fig. 1, but the data obtained for this composition are listed in Table 4), which formally indicates a large excess of "overstoichiometric" oxygen, but it can be attributed to the specific microstructure of the sample as well.

Hydrogen uptake in the medium-temperature region (440–600°C). According to our calculations, this region corresponds to the reduction process $Mn^{4+} \longrightarrow Mn^{2+}$, which means oxygen elimination from the coordination sphere of the Mn_{Ca}^{4+} cations. It is clear from Fig. 1 that the T_{max} values depend on x. Let us consider the data (Tables 1–3) obtained for this temperature region in greater detail.

The substitution of calcium for lanthanum up to a small extent of x = 0.2 shifts the peaks in this region to higher temperatures and raises the hydrogen uptake (Table 4) by increasing the Mn_{Ca}^{4+} fraction. However, the general situation remains the same: the hydrogen uptake value corresponds to the reduction process $Mn^{4+} \longrightarrow Mn^{2+}$ in the perovskite $La_{0.8}Ca_{0.2}MnO_{3+\delta}$. Thus, the process $Mn^{4+} \longrightarrow Mn^{2+}$ in these samples does not affect the bulk perovskite structure.

The samples with medium extents of substitution (x = 0.4, 0.6), which have a complicated phase composition (MC series) or are microheterogeneous (ceramic series), are characterized by complicated TPR curves between 400 and 700°C (peak with T_{max} ~ 530–600°C). The TPR peaks due to the process $Mn^{4+} \longrightarrow Mn^{2+}$ are split for the MC series and broadened for the ceramic series (Fig. 1). The splitting of the peaks may be due to the fact that these samples are not single phases (Tables 2, 3). Apparently, calcium-rich phases ($CaMnO_{3-x}$) are reduced at lower temperatures. According to formal calculations, the Mn^{4+} content of these samples is as high as 58–67% for T_{calcin} = 1100°C and 72–80% for T_{calcin} = 900°C.

The highly substituted samples (x = 0.8, 1.0) are characterized by hydrogen uptake at ~350–550°C (peaks with T_{max} = 400–490°C). According to our calculations, the amount of hydrogen (Table 4) consumed by the x = 0.8 sample calcined at 1100°C corresponds to the reduction process $Mn^{4+} \longrightarrow Mn^{3+}$ taking place in the perovskite $La_{1-x}Ca_xMnO_{3+\delta}$ and to the process $Mn^{4+} \longrightarrow Mn^{2+}$ in the perovskite $CaMnO_{3-x}$. According to x-ray diffraction data, the x = 1 samples of the three series are two-phase systems consisting of the perovskite $CaMnO_{3-x}$ and the braunmillerite-like phase $Ca_2Mn_2O_5$ (in which all manganese is in the Mn^{3+} state). Therefore, the reduction process $Mn^{4+} \longrightarrow Mn^{2+}$ in these samples occurs only in the $CaMnO_{3-x}$ phase and proceeds to the full extent, causing perovskite decomposition into the starting oxides (CaO and MnO). Note that, for the x = 1 samples, Tables 1, 3 present the ratio of the perovskite $CaMnO_{3-x}$ to the braunmillerite $Ca_2Mn_2O_5$ derived from the ratio of the first and second TPR peaks. The information concerning the percentage ratio of these phases is interesting because these phases cannot be separated by the DD method. A plausible explanation for the deduction that manganese is reduced less deeply ($Mn^{4+} \longrightarrow Mn^{3+}$) is that the electroneutrality of the sample is ensured by the formation of both Mn^{4+} cations and oxygen vacancies.

Hydrogen uptake in the high-temperature region. The amounts of hydrogen reacting with the samples in this temperatures region correspond to the process $Mn^{3+} \longrightarrow Mn^{2+}$. The TPR peak positions (T_{max}) depend on the composition of the catalyst (Fig. 1, Tables 1–4). For the x = 0 sample activated at 1100°C for 10 min, the $Mn^{3+} \longrightarrow Mn^{2+}$ process begins at 700°C, while the same process in calcium manganite is complete at this temperature. Thus, bulk reduction accompanied by the decomposition of the perovskite phase takes place in this temperature region. As the calcium content of the sample is raised, the onset of this process shifts to lower temperature and the process proceeds to the full extent. As follows from our data, the Mn^{3+} fraction derived from the high-temperature hydrogen uptake peaks decreases with increasing calcium content. This is consistent with the deeper reduction process $Mn^{4+} \longrightarrow Mn^{2+}$ taking place at low temperatures. The Mn^{3+} fraction is close to 100% only in the x = 0.8 samples, indicating that these samples are reduced less deeply in the low-temperature region. For the MC samples of intermediate compositions, the TPR peaks are split and broadened. By analogy with the medium-temperature region, this effect can be attributed to the heterogeneity of the system. It is interesting that the single-phase ceramic samples with x = 0.4 and 0.6 are also characterized by split and broadened TPR peaks in the high-temperature region. This effect is most likely due to the nonuniformity or microheterogeneity of the samples (core–shell structures). However, this point needs further investigation.

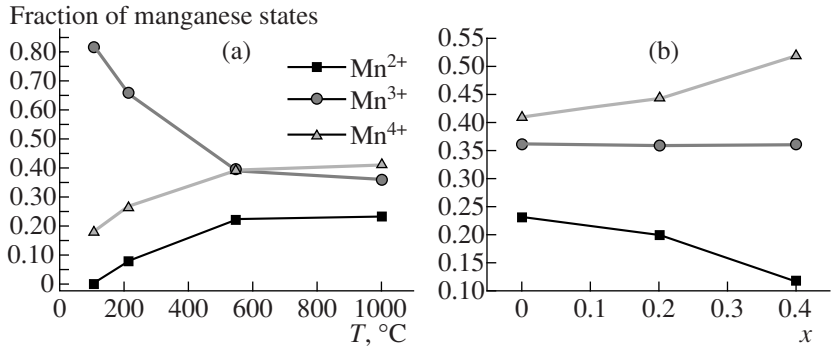

Fig. 4. Fractions of different states of manganese in $La_{1-x}Ca_xMnO_{3+y}$ as a function of (a) temperature and (b) the calcium stoichiometry x at $T = 1000$°C (according to [22]).

The ratio of Mn^{4+} to Mn^{3+} derived from the low- and high-temperature TPR peaks indicates, in some cases, the presence of another weakly bound form of oxygen. This form can lead to overestimation of the thus-determined Mn^{4+} fraction. It can only be hypothesized that this form of oxygen is either extra "oxygen planes" or oxygen at interblock boundaries.

Thus, based on TPR data, we distinguish the following four forms of oxygen with different reactivities in the $La_{1-x}Ca_xMnO_{3+\delta}$ perovskites: surface oxygen, which is the most reactive; lattice oxygen bound to Mn^{3+}; and two forms of oxygen bound to Mn^{4+} (one is the "overstoichiometric" oxygen O_δ, which is present even in unsubstituted lanthanum manganite, and the other is oxygen bound to those Mn^{4+} ions that resulted from the introduction of calcium). Furthermore, our data indicate that oxygen located at interblock boundaries—another form of oxygen—exists in microheterogeneous samples.

Effect of the Synthesis Conditions

Table 4 lists TPR maximum positions and the hydrogen uptake values for the corresponding peaks for different synthesis methods, specifically, different calcination temperatures and times. As the calcination temperature and time are increased, the maxima of the reduction peaks shift to higher temperatures. The total hydrogen uptake for each sample can be slightly higher than the sum of the hydrogen uptakes at the separate peaks because of the contribution from the reduction of impurity Mn_3O_4 (this process can take place in the temperature range of 400–600°C and should be taken into account when the amount of this oxide is >1–2%). It is clear from our data that the lower the calcination temperature, the better the reducibility of the resulting perovskite. Accordingly, the hydrogen uptake decreases with increasing calcination temperature, indicating a decline in the reactivity of oxygen. These changes are not directly associated with the decreasing specific surface area. They are more likely caused by changes in the real structure or microstructure of the oxide. According to SIMS data [15], the surface of lower temperature samples can be enriched with oxygen and there can be surface segregation of calcium at shorter heat-treatment times (that is, for the MC series). According to our TPR data, the MC samples calcined at 900°C have larger proportions of overstoichiometric oxygen O_δ than the MC samples calcined at 1100°C or the ceramic samples. This finding is in exact agreement with SIMS data [15]. Thus, the lower the synthesis temperature, the higher the Mn^{4+} content of the resulting material (Tables 1, 2).

DISCUSSION

A comparison between our data and the literature data available on the reduction of the $La_{1-x}Ca_xMnO_{3+\delta}$ system with hydrogen shows the coincidence of the most general trends: as the calcium content of the system is increased, the overall reducibility of the system increases and the maxima of the TPR peaks shift to lower temperatures. However, we found that the hydrogen uptake in the medium-temperature range exceeds the value necessary for the process $Mn^{4+} \longrightarrow Mn^{3+}$ to occur, contrary to what was reported by Ponce et al. [18].

We attribute the increase of the hydrogen uptake in the medium-temperature range to the occurrence of the deeper manganese reduction process $Mn^{4+} \longrightarrow Mn^{2+}$, as was done in the case of strontium-substituted manganites [16]. Our data disagree with the explanation of this effect in the framework of the less deep reduction model ($Mn^{4+} \longrightarrow Mn^{3+}$) [22] (in which this effect is attributed to the reduction of the extra Mn^{4+} cations resulting from the thermally induced disproportionation of part of the Mn^{3+} cations into Mn^{4+} and Mn^{2+} above 400°C (Fig. 4a)). We observed that the Mn^{4+} and Mn^{3+} contents vary almost symbatically with the calcium content, while Stevenson [22] established that, as calcium is progressively substituted for lanthanum, the Mn^{3+} fraction remains almost unchanged (~36%), the Mn^{4+} fraction grows, and the Mn^{2+} fraction decreases

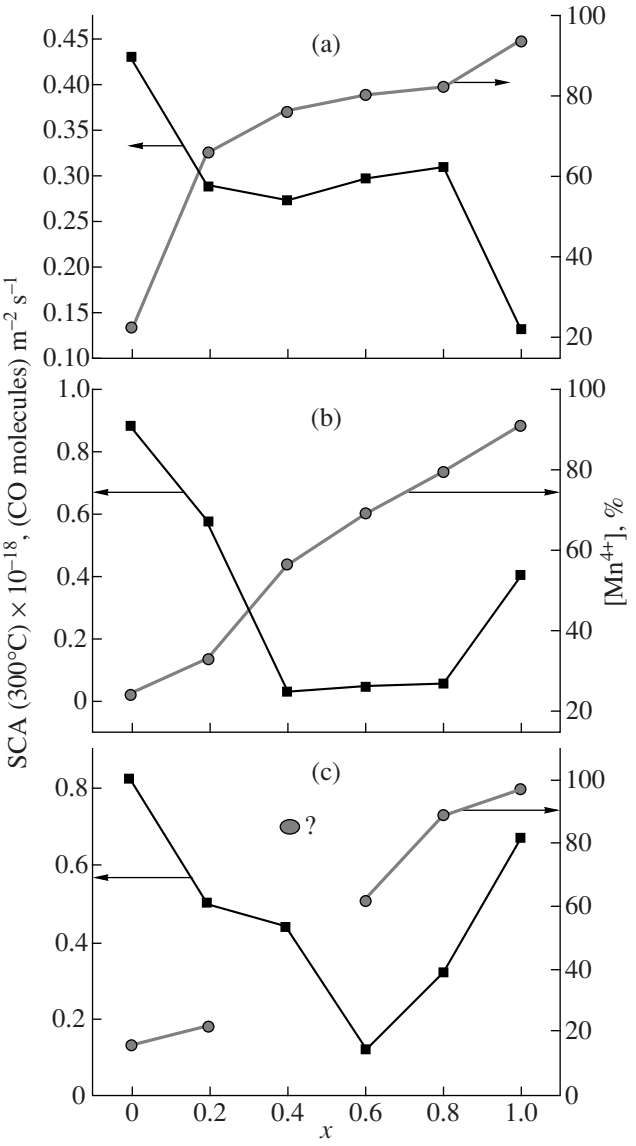

Fig. 5. Mn^{4+} content and CO oxidation rate at T_{test} = 300°C as a function of x for (a, b) mechanochemical samples (T_{calcin} = (a) 900 and (b) 1100°C) and (c) ceramic samples.

(Fig. 4b). However, from TPR data alone, it is difficult to deduce whether the Mn^{2+} cations appearing below 500°C result from disproportionation or from the deep reduction process hypothesized by us. This can be done by in situ methods capable of elucidating the distribution of different manganese cations.

The deeper manganese reduction observed in this study may have different causes, including the larger specific surface area, the specific particle microstructure, and the higher reactivity of oxygen of our samples. The same features may cause the difference between the reactivities of the ceramic and MC sample series since increasing the calcination temperature and time

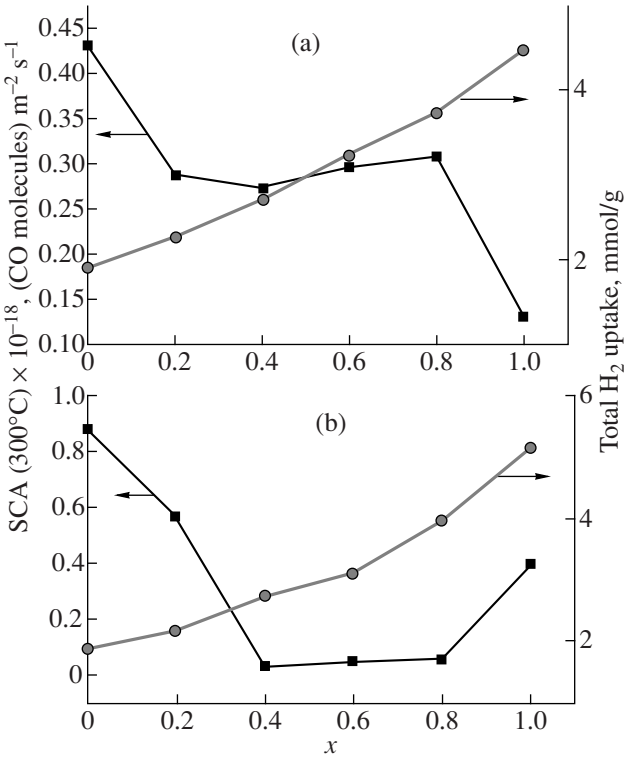

Fig. 6. CO oxidation rate at T_{test} = 300°C and total hydrogen uptake as a function of x for mechanochemical samples calcined at (a) 900 and (b) 1100°C.

leads to a decrease in the hydrogen uptake (TPR peak intensity) in all the temperature regions examined.

Thus, we established that the reactivity of the different forms of oxygen present in substituted perovskite manganites depends both on the chemical composition of the sample and on the synthesis conditions.

A simultaneous analysis of TPR and CO oxidation activity data demonstrated that the changes in SCA are not correlated with the Mn^{4+} content (Fig. 3). Likewise, there is no correlation between SCA and the total hydrogen uptake (Table 4, Fig. 6). However, as was noted above, the dependence of the hydrogen uptake in the low-temperature region on the sample composition is similar to the dependence of catalytic activity on the sample composition (Fig. 5). The existence of a correlation between the catalytic activity of the $La_{1-x}Ca_xMnO_{3+\delta}$ system in CO oxidation and the amount of the most reactive surface oxygen suggests that the leading role in CO oxidation on perovskites is played by the weakly bound surface forms of oxygen. This deduction is quite consistent with the stepwise mechanism suggested for perovskites involved in catalytic CO oxidation.

REFERENCES

1. Kharton, V.V., Yaremchenko, A.A., and Naumovich, E.N., *J. Solid State Chem.*, 1999, vol. 3, p. 303.

2. Tejuca, L.G., Fierro, J.L.G., and Tascon, J.M.D., *Adv. Catal.*, 1989, vol. 36, p. 237.
3. Baran, E.J., *Catal. Today*, 1990, vol. 8, no. 2, p. 133.
4. Wollan, E.O. and Koehler, W.C., *Phys. Rev.*, 1955, vol. 100, p. 545.
5. Ramirez, A.P., *J. Phys.: Condens. Matter*, 1997, vol. 9, no. 1, p. 8171.
6. Coey, J.M.D., Viret, M., von Molnar, S., *Adv. Phys.*, 1999, vol. 48, no. 2, p. 167.
7. Seiyama, T., *Catal. Rev. Sci. Eng.*, 1991, vol. 34, no. 4, p. 281.
8. Yamazoe, N. and Teraoka, V., *Catal. Today*, 1990, vol. 8, no. 2, p. 175.
9. Fierro, J.L.G., *Catal. Today*, 1990, vol. 8, no. 2, p. 153.
10. Yue Wu, Tao Yu, and Bo-Sheng Dou, *J. Catal.*, 1989, vol. 120, p. 88.
11. Tabata, K. and Misono, M., *Catal. Today*, 1990, vol. 8, no. 2, p. 249.
12. Rao, C.N.R., Chittham, A.K., and Mahesh, R., *Chem. Mater.*, 1996, vol. 8, p. 2421.
13. Tamaitsu, H., Wada, K., Kaneko, H., and Yamamura, H., *J. Am. Ceram. Soc.*, 1992, vol. 75, p. 401.
14. Majewski, P., Epple, L., Rozumek, M., Shluckwerder, H., and Aldinger, F., *J. Mater. Res.*, 2000, vol. 15, no. 5, p. 1161.
15. Isupova, L.A., Tsybulya, S.V., Kryukova, G.N., Alikina, G.M., Boldyreva, N.N., Yakovleva, I.S., Ivanov, V.P., and Sadykov, V.A., *Solid State Ionics*, 2001, vols. 141–142, p. 417.
16. Ciambelli, P., Cimino, S., De Rossi, S., Faticanti, M., Lisi, L., Minelli, G., Pettiti, I., Porta, P., Russo, G., and Turco, M., *Appl. Catal., B*, 2000, vol. 24, p. 243.
17. Cimino, S., Lisi, L., Pirone, R., Russo, G., and Turco, M., *Catal. Today*, 2000, vol. 59, p. 19.
18. Ponce, S., Pena, M.A., and Fierro, J.L.G., *Appl. Catal., B*, 2000, vol. 24, p. 193.
19. Isupova, L.A., Yakovleva, I.S., Alikina, G.M., Rogov, V.A., and Sadykov, V.A, *Kinet. Katal.*, 2005, vol. 46, no. 5, p. 773 [*Kinet. Catal.* (Engl. Transl.), vol. 46, no. 5, p. 729].
20. Sadykov, V.A., Isupova, L.A., and Yakovleva, I.S., *React. Kinet. Catal. Lett.*, 2004, vol. 81, no. 2, p. 393.
21. Royer, S., Alamdari, H., and Kalyaguine, S., *Appl. Catal., B*, 2005, vol. 58, p. 273.
22. Stevenson, J.W., *J. Solid State Chem.*, 1993, vol. 102, p. 175.